Regulation of Photoactivation in Vertebrate Short Wavelength Visual Pigments: Protonation of the Retinylidene Schiff Base and a Counterion Switch

Lavoisier S. Ramos,[‡,§] Min-Hsuan Chen,[§,||] Barry E. Knox,*[,||] and Robert R. Birge*[,‡]

Departments of Chemistry and of Molecular and Cell Biology, University of Connecticut, Storrs, Connecticut 06269, and Departments of Biochemistry and Molecular Biology and of Ophthalmology, SUNY Upstate Medical University, Syracuse, New York 13210

Received January 23, 2007; Revised Manuscript Received March 12, 2007

ABSTRACT: *Xenopus* violet cone opsin (VCOP) and its counterion variant (VCOP-D108A) are expressed in mammalian COS1 cells and regenerated with 11-*cis*-retinal. The phototransduction process in VCOP-D108A is investigated via cryogenic electronic spectroscopy, homology modeling, molecular dynamics, and molecular orbital theory. The VCOP-D108A variant is a UV-like pigment that displays less efficient photoactivation than the mouse short wavelength sensitive visual pigment (MUV) and photobleaching properties that are significantly different. Theoretical calculations trace the difference to the protonation state of the nearby glutamic acid residue E176, which is the homology equivalent of E181 in rhodopsin. We find that E176 is negatively charged in MUV but neutral (protonated) in VCOP-D108A. In the dark state, VCOP-D108A has an unprotonated Schiff base (SB) chromophore ($\lambda_{max} = 357$ nm). Photolysis of VCOP-D108A at 70 K generates a *bathochromic* photostationary state ($\lambda_{max} = 380$ nm). We identify two *lumi* intermediates, wherein the transitions from *batho* to the *lumi* intermediates are temperature- and pH-dependent. The *batho* intermediate decays to a more red-shifted intermediate called *lumi* I. The SB becomes protonated during the *lumi* I to *lumi* II transition. Decay of *lumi* II forms *meta* I, followed by the formation of *meta* II. We conclude that even in the absence of a primary counterion in VCOP-D108A, the SB becomes protonated during the photoactivation cascade. We examine the relevance of this observation to the counterion switch mechanism of visual pigment activation.

The visual pigments of the vertebrate retina are classified into five different families: M/LWS (mid and long wavelength sensitive), SWS1 (short wavelength sensitive 1), SWS2 (short wavelength sensitive 2), RH1 (rhodopsins), and RH2 (rodlike pigments) (*1*−*4*). Each family of opsins mediates sensitivity in a specific region of the spectrum. All vertebrate opsins are heptahelical membrane proteins found in the outer segment of the photoreceptor cells. The vertebrate opsins have a lysine residue in the seventh transmembrane helix to which an 11-*cis*-retinal chromophore is covalently attached (K296 in rhodopsin and K291 in VCOP) via a Schiff base (SB)[1] linkage. In all vertebrate opsins, except for some SWS1 pigments, the SB is protonated. A negatively charged residue, also called the primary counterion, in transmembrane helix 3 (E113 in rhodopsin, E108 in MUV, and D108 in VCOP) stabilizes the protonated SB (PSB). One photoactivation model for rhodopsin, called the counterion switch model, proposes that another residue in extracellular loop 2 (E181 in rhodopsin and E176 in both VCOP and MUV) serves as a counterion and is involved in the activation of rhodopsin (*5*, *6*). The counterion switch occurs during a conformational change, which moves E181 closer to, and E113 farther from, the SB of rhodopsin. Our previous studies show that the UV pigments also include a counterion switch (*6*−*8*). Analogous to rhodopsin, the counterion switch from the primary counterion, E108, to E176 in MUV occurs during the *lumi* to *meta* I transition.

The SWS1 pigments have been the focus of our research because little is known about the chromophore−opsin interactions and unique photoactivation properties in these cone pigments. The SWS1 family of vertebrate visual pigments has an absorption maximum between 350 and 450 nm and is divided into two groups: those that absorb in the 400−440 nm range (blue/violet) and those that absorb in the 350−390 nm range (UV). From our previous studies, we have shown that some of the SWS1 pigments have an unprotonated SB, and this explains the wide energy gap between the violet/blue cones and the UV cones (*7*, *8*). Cryogenic UV−vis spectroscopy reveals the photoactivation sequences of the two SWS1 pigments, the *Xenopus* violet cone pigment (VCOP; $\lambda_{max} = 427$ nm) and the mouse UV cone pigment (MUV; $\lambda_{max} = 360$ nm). VCOP has a PSB

* To whom correspondence should be addressed. R.R.B.: telephone, (860) 486-6720; fax, (860) 486-2981; e-mail, rbirge@uconn.edu. B.E.K.: telephone, (315) 464-8719; fax, (315) 464-8750; e-mail, knoxb@upstate.edu.

‡ University of Connecticut.

§ These authors contributed equally to this work.

|| SUNY Upstate Medical University.

[1] Abbreviations: VCOP, *Xenopus laevis* violet cone opsin; MUV, mouse UV cone opsin; SB, Schiff base; PSB, protonated Schiff base; HEPES, *N*-(2-hydroxyethyl)piperazine-*N*′-2-ethanesulfonic acid; PSS, photostationary state; *batho*, *lumi* I, *lumi* II, *meta* I, and *meta* II, discrete thermal intermediates in the photobleaching pathway of visual pigments; VMD, visual molecular dynamics; MNDO-PSDCI, modified neglect of differential overlap with partial single- and double-configuration interaction.

10.1021/bi700138g CCC: $37.00
Published on Web 04/18/2007 PAGE EST: 11

chromophore in the dark, and its photoactivation pathway is remarkably similar to that observed in rhodopsin.

Fourier transform infrared spectroscopy (FTIR) studies show that MUV has an unprotonated SB, which explains the significant hypsochromic shift in its absorption maximum in the dark state compared to that of VCOP (*8*). Our homology model of MUV predicts that the counterion (E108) is sufficiently close to extract the proton from the SB chromophore which provides insight into why MUV has an unprotonated SB chromophore in the dark state. Among the SWS1 pigments, positions 81, 85, and 88 (86, 90, and 93, respectively, in rho numbering) were identified as key residues that modulate the environment of the SB to favor a charged (protonated) or a neutral chromophore (*9*−*13*). Besides the protonation state of the SB, the relative position of the counterion with respect to the SB and the arrangement of the residues in the chromophore binding pocket contribute to the overall mechanism of spectral tuning in SWS1 pigments.

To understand the electrostatic interactions between the chromophore and the surrounding key residues, variants of the pigment were characterized by using UV−vis spectroscopy. Site-directed mutagenesis has shown that the D108 residue serves as a primary counterion in VCOP and the removal of this charged residue results in a dramatic change in the pK_a of the SB (*14*). In previous studies, we have replaced the aspartic acid residue at position 108 with similarly sized and neutral residues, such as glutamine and asparagine. D108Q did not bind retinal, while D108N (λ_{max} = 365 nm) exhibits a significant decrease in the level of binding with 11-*cis*-retinal. Replacing the aspartic acid at position 108 with a neutral residue, such as alanine, gave a blue-shifted absorption maximum. Like that of MUV, the absorption maximum of VCOP-D108A (λ_{max} = 357 nm, 25 °C) suggests that it has an unprotonated SB. The VCOP-D108A pigment exhibits a significantly long-lived *meta* II intermediate but is incapable of activating bovine rod transducin in the dark (*14*).

In this study, the photobleaching pathway of VCOP-D108A is characterized and the possible role of E176 is investigated. In this report, we show that the earlier intermediates of the photoactivation sequence of VCOP-D108A are significantly affected by the removal of a charged residue at position 108. However, neutralizing the primary counterion in VCOP does not hinder the formation of an activated opsin, *meta* II. We conclude that the protonation state of E176 plays an important role in the formation kinetics and properties of the early intermediates, and our results provide new insights into the nature and relevance of the counterion switch mechanism.

MATERIALS AND METHODS

Site-Directed Mutagenesis and Visual Pigment Expression and Purification. The epitope-tagged VCOP plasmids used for site-directed mutagenesis and protein expression have been described previously (*14*). The mutants were expressed in COS1 cells by transient transfection, purified by immunoaffinity chromatography, and analyzed as described in ref *14*. Pigments were eluted in buffer Y1 [50 mM HEPES, 140 mM NaCl, and 3 mM $MgCl_2$ (pH 6.6)] with 0.1% *N*-dodecyl β-D-maltoside and 20% glycerol.

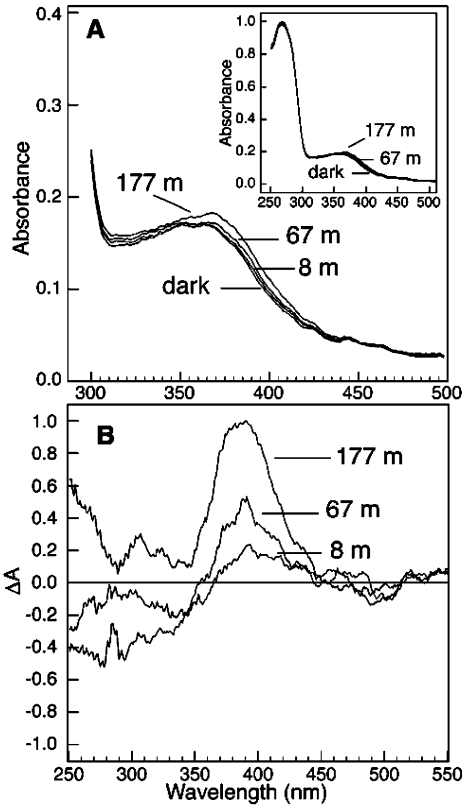

FIGURE 1: Photochemistry of VCOP-D108A (pH 6.8) at 70 K. The formation of *batho* was observed during the illumination of the pigment with 310 nm light. (A) Spectra of the pigment after successive illumination at 70 K. (B) Difference spectra of illuminated minus dark VCOP-D108A.

Cryogenic Electronic Spectroscopy. Samples were prepared in 67% glycerol, 0.05% *N*-dodecyl β-D-maltoside, and 1× buffer Y [50 mM HEPES, 140 mM NaCl, and 3 mM $MgCl_2$ (pH 6.8)]. All experiments for studies at 70−230 K were performed in a helium-refrigerated cryostat (APD, Inc.) coupled to a Cary 50 UV−vis spectrophotometer. For studies at 230−280 K, samples were placed in a temperature-controlled sample holder inside the Cary 5000 UV−vis spectrometer. To generate the photostationary states, samples were illuminated with a Photomax system equipped with a 200 W arc lamp and a monochromator (Oriel, Stratford, CT). The samples were illuminated until no further spectral changes could be observed.

To determine the chromophore conformation, retinal oximes were extracted and analyzed using HPLC and methods reported previously (*15*).

Homology Models and Computational Methods. Protein modeling was performed using molecular dynamics methods modified from those of Schulten and colleagues (*16*). Homology models of VCOP were constructed using the crystal structure of rhodopsin (PDB entry 1U19) (*17*). Homology models of rhodopsin, VCOP, and VCOP-D108A were constructed using Modeler (*18*). Thirty-six internal hydration water molecules were introduced using the rhodopsin crystal structure and those predicted by DOWSER (*19*). The complete protein homology model with internal hydration water molecules was minimized in NAMD (*20*) for 4000 steps. The membrane was included in the model using 1-palmitoyl-2-oleoylphosphatidylcholine (POPC) molecules to simulate the unsaturated phospholipids of the outer

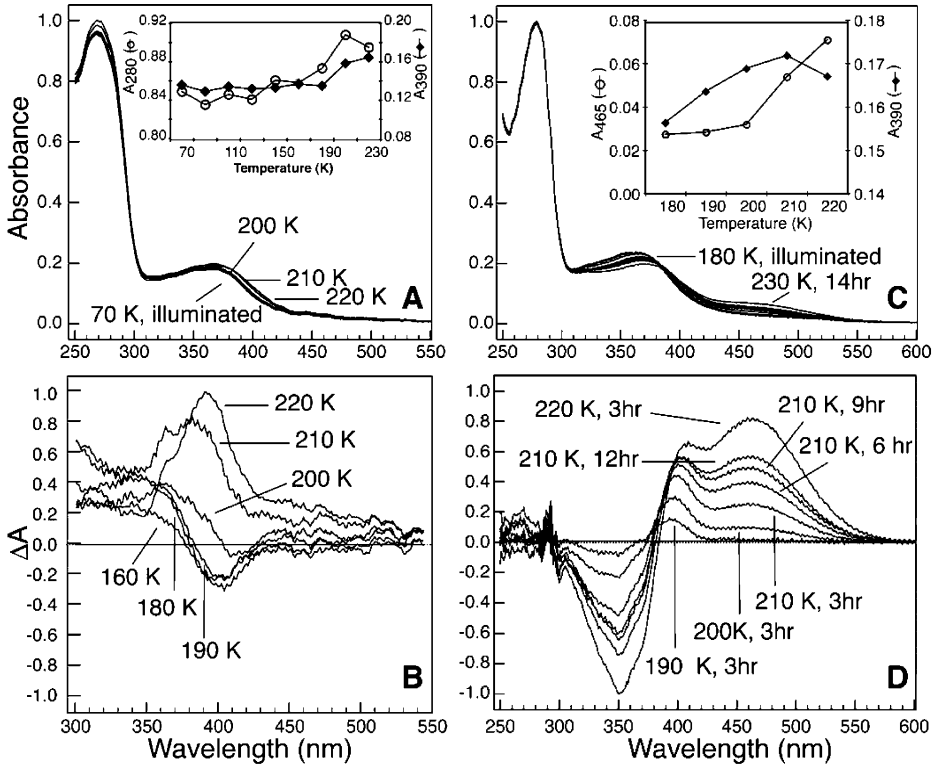

FIGURE 2: Thermal decay of the photostationary state (PSS368) formed at 70 K. The formation of *lumi* I and *lumi* II intermediates is observed at 190 and 200 K, respectively. (A) After illumination at 70 K, the sample was warmed in increments of 10 K, equilibrated for 1 h, and cooled to 70 K before the spectrum was recorded. (B) Difference spectra of the warmed sample minus the PSS368 spectrum, from the data set in panel A. (C) After illumination at 180 K, the sample was warmed in increments of 10 K and equilibrated for several hours (as indicated). (D) Difference spectra of the warmed sample minus the PSS368 spectrum, from the data in panel C. The insets in panels A and C show plots of the absorbance changes monitored at 280, 390, and 465 nm during the temperature ramping.

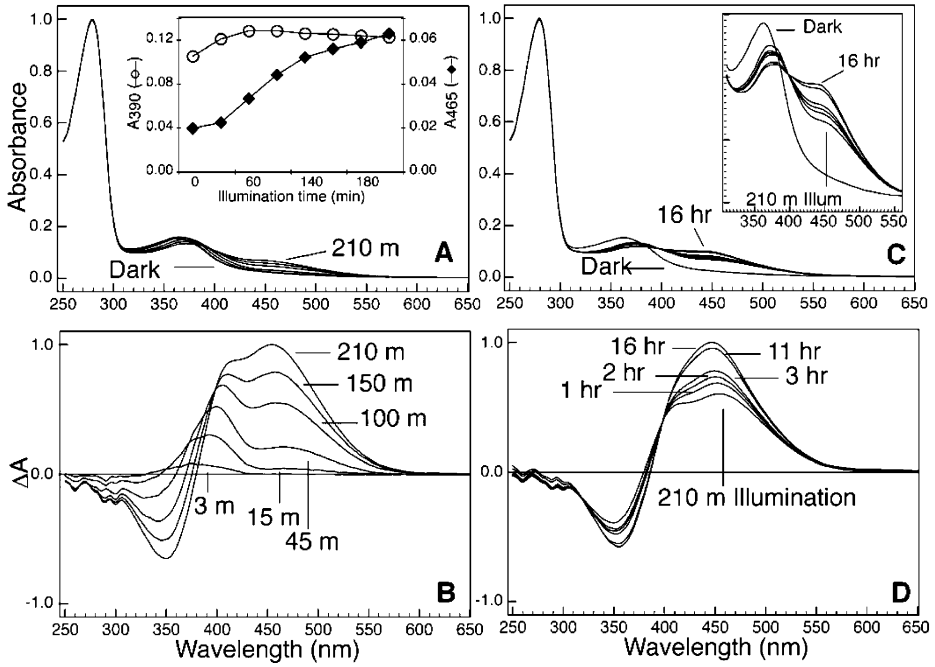

FIGURE 3: Formation of the *lumi* I, *lumi* II, and *meta* I intermediates. (A) VCOP-D108A (pH 6.8) was illuminated with 310 nm light at 233 K for several hours until no spectral change was observed. The inset in panel A shows a plot of absorbance changes monitored at 390 and 465 nm during the illumination, corresponding to the formation of *lumi* I and *lumi* II, respectively. (B) Difference spectra of the illuminated sample minus the dark state at 233 K. (C) Formation of *meta* I was observed when the sample was further equilibrated for several hours in the dark at 233 K after illumination. The inset in panel C shows an expanded scale showing the shift of the chromophore band to 440 nm. (D) Difference spectra of the illuminated sample minus the dark VCOP-D108A pigment.

segment (*21*). A lipid box was built using VMD (90 Å × 90 Å) and the protein embedded by using VMD. Lipid molecules overlapping with the protein were removed, and the final model contained 169 POPC molecules. A short molecular dynamics (120 ps) simulation was performed on the protein−membrane model to relax the protein−lipid

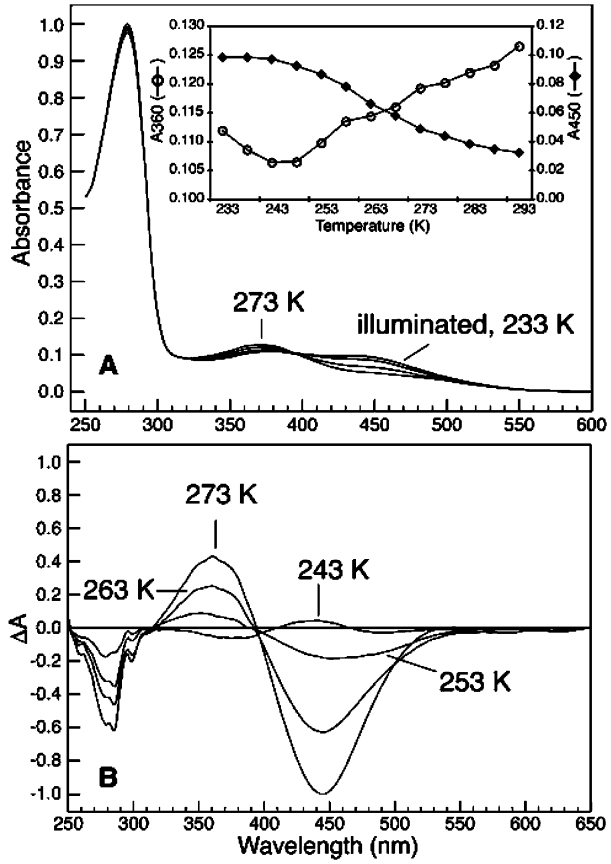

FIGURE 4: Formation and decay of later intermediates of VCOP-D108A. (A) After illumination with 310 nm light at 233 K, the sample was warmed in increments of 5 K. The inset in panel A shows a plot of absorbance changes monitored at 360 and 450 nm. The *meta* I starts to decay to the *meta* II intermediate at 253 K. (B) Difference spectra of the warmed sample minus the illuminated sample at 233 K.

interface. The system was then solvated with water molecules (TIP3) by using VMD. The fully solvated system had dimensions of 90 Å × 90 Å × 100 Å and contained 13 542 water molecules. After solvation, 38 sodium and chloride ions were added to neutralize the system, and these were manually redistributed on the basis of the surface potential map generated by GRASP (*22*). All molecular dynamic simulations were carried out with full PME calculations for electrostatic interactions. To ensure that the system was relaxed systematically, simulations were carried out using a Langevin bath as follows: 25 ps with the protein fixed, 25 ps with the entire protein harmonically constrained, 25 ps with the peptide backbone harmonically constrained, 25 ps with α-carbons harmonically constrained, and finally 25 ps with only the retinal constrained. NPT ensemble (constant pressure and temperature) simulation was then performed for 2 ns. The same procedure was followed for the simulation of earlier intermediates of the visual pigments with an all-*trans*-retinal chromophore.

Following molecular dynamics, the chromophore was optimized by using the PM3 Hamiltonian within MOZYME (*23*−*25*) as implemented within Chem3D and MopacUltra (CambridgeSoft, Cambridge, MA). During the optimization of the chromophore, only the chromophore and the side chain of Lys 291 were allowed to move while the rest of the protein was held fixed. Optimization of the chromophore eliminates minor flaws in the chromophore geometry that lead to unrealistic transition energy calculations. The photophysical properties of the chromophore were calculated by using modified neglect of differential overlap with partial single- and double-configuration interaction (MNDO-PSDCI) molecular orbital theory (*26*) and parametrizations as described previously (*27*, *28*). The PM3 Hamiltonian was selected for all the calculations because it routinely yields the most realistic transition energies and oscillator strength. All the calculations reported here assumed a 6-*s*-*cis* conformation of the β-ionone ring of the chromophore, and test calculations verified that this conformation has an energy lower than that of the 6-*s*-*trans* conformation.

RESULTS

Formation of Early Intermediates. Replacing the residue of VCOP at position 108 with a neutral residue results in a hypsochromic shift in the absorption maximum from 425 to 357 nm. The absorption maximum red shifts to 363 nm when VCOP-D108A is cooled to 70 K. The pigment was illuminated with 310 nm light, forming a bathochromic photostationary state as shown in Figure 1. The photolysis of the pigment at 70 K resulted in a 5 nm red shift in the chromophore peak from 363 to 368 nm. The illumination was carried out for several hours to ensure that the photostationary state (PSS368) was achieved with maximal formation of a *batho* intermediate. Retinal extraction of PSS368 in VCOP-D108A indicated a mixture of retinal isomers: 75% all-*trans*, 12% 11-*cis*, and 13% 9-*cis* isomers.

The temperature of the *batho* photostationary state was gradually increased in increments of 5 K and displayed no spectral shift from 70 to 180 K (Figure 2A,B). To avoid artifacts associated with temperature-dependent baseline shifts, the sample was cooled back to 70 K prior to collection of the spectra. Further warming of the pigment subsequently shifted the absorption maximum toward the red and formed the next thermally stable intermediate at 190 K. The difference spectra show a positive band at 390 nm together with a small increase in the absorbance of the opsin peak at 280 nm. The temperature of the sample was increased to 200 K, and this generated two bands located in the 390 and 450 nm region. To look closely at the formation of the 390 nm peak and to probe the nature of the absorbance in the 450 nm region, we performed another set of experiments. As shown in panels C and D of Figure 2, the illuminated sample was equilibrated at 190, 200, and 210 K for an extended period of time to achieve more complete conversion to the appropriate, thermally stable intermediate. Similar to what was observed in the first set of data shown in Figure 2A, the 390 nm band formed when the temperature of the sample was at 190 K. The difference spectra in Figure 2D show a negative change in absorbance at 350 nm, which is due to the decay of the *batho* VCOP-D108A. The two positive bands located at 390 and 470 nm correspond to the formation of two intermediates, which we label, in order of formation, *lumi* I and *lumi* II, respectively.

Formation of Later Intermediates. The later intermediates of the photoactivation sequence of VCOP-D108A were studied at higher temperatures (>230 K). Illumination of the pigment at 233 K (Figure 3) resulted in the formation of a mixture of the two intermediates (λ_{max} = 394 nm, and λ_{max} = 460 nm). The inset of Figure 3A shows that the increase

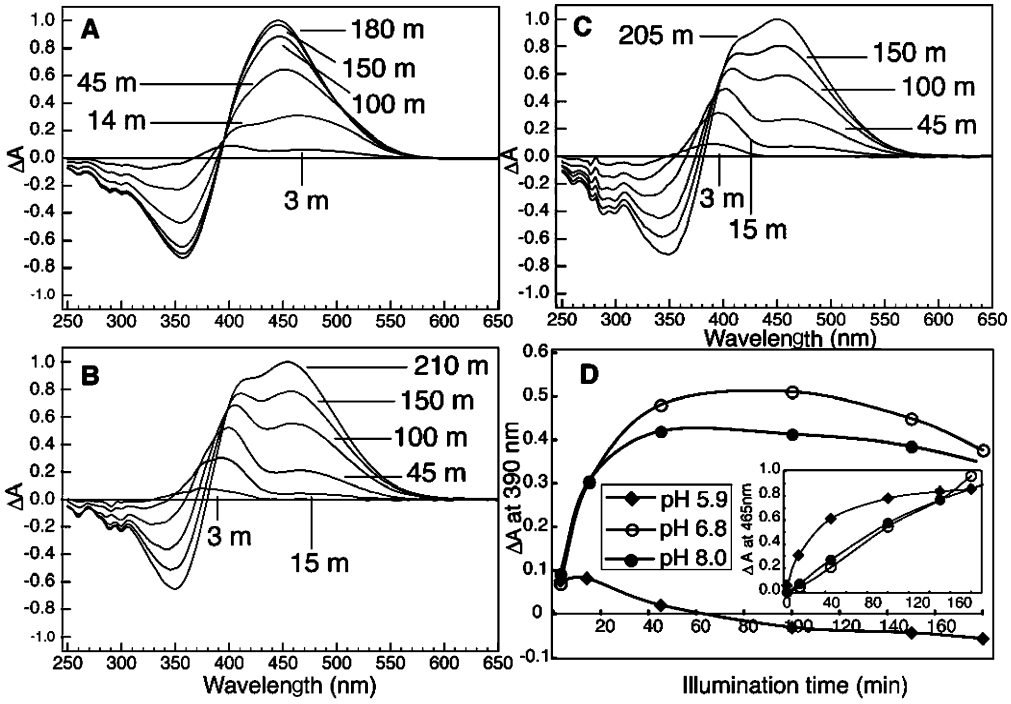

FIGURE 5: Photobleaching difference spectra of VCOP-D108A at (A) pH 5.9, (B) 6.8, and (C) 8.0. The spectra were generated by illuminating the sample with 310 nm light at 233 K for several hours as indicated (in minutes). (D) The absorbance changes at 390 nm at different pHs are plotted vs the illumination time. The inset in panel D shows a plot of the absorbance changes at 465 nm.

in the absorbance at 390 nm ended after illumination for 40 min, while an increase in the absorbance at 465 nm band was observed after illumination for 30 min. The sample was kept in the dark after illumination for a few hours, and this resulted in a spectral shift centered at 450 nm as shown in the difference spectra in Figure 3D. This 450 nm band is associated with the formation of the *meta* I intermediate. The *meta* I formation in VCOP-D108A is observed at a slightly lower temperature compared to that of VCOP. With a gradual increase in temperature, the absorption band at 450 nm slowly decreased while the band at 360 nm gained intensity, associated with the decay of *meta* I and the formation of *meta* II (Figure 4).

To investigate the effect of the pH environment on the photoactivation sequence of VCOP-D108A, the pigment was suspended in buffers at pH 5.9, 6.8, and 8.0 as shown in Figure 5. The absorption maximum of VCOP-D108A in the dark was unaffected by the pH change. The same photoactivation intermediates were formed under all three pH conditions. However, when the pH was lowered to 5.9, the formation of the intermediates at 233 K was faster compared to that at pH 6.8 and 8.0. *Lumi* I formation was already observed after illumination for 3 min. After 45 min, there was little *lumi* I remaining and most of the pigment was *lumi* II. For samples at pH 6.8 and 8.0, the formation of *lumi* II was observed only after illumination for 14 min.

Derivation of the Spectra of the Intermediates. The calculated electronic spectra of the pure intermediates in Figure 6 were generated from the spectra of temperature-trapped intermediates via spectral deconvolution. The dark state and *batho* intermediates of VCOP-D108A are comparable to those of MUV. In contrast to other visual pigments, the *batho* intermediate of VCOP-D108A is followed by a red-shifted intermediate, *lumi* I. The absorption maxima of *lumi* II and *meta* I are red-shifted compared to that of the PSB in solution, indicating that the SB at these intermediates is protonated. Analogous to what is observed in *meta* II of VCOP and MUV, the absorption maximum of *meta* II in VCOP-D108A is ~370 nm, characteristic of an unprotonated SB.

DISCUSSION

Previous studies on the rhodopsin counterion variant, E113Q, showed a pH dependence of the absorption maximum of the pigment (*29*, *30*). The protonation state of the chromophore SB in E113Q-rhodopsin is dependent on the pH in the range of 4−9, whereas VCOP and VCOP-D108A are pH-independent. VCOP-D108A maintains an absorption maximum of 357 nm in this pH range (pH 4−9), which implies that the pK_a values of the retinal Schiff base linkages are outside of the investigated pH range (*14*).

Photoactivation Sequence of VCOP-D108A. The VCOP-D108A counterion variant is a violet sensitive pigment converted into a UV-like pigment, which has an unprotonated SB in the dark. In MUV, the SB is unprotonated but the counterion (E108) in transmembrane 3 is still present. The counterion in VCOP is D108, which has a carbon linkage one atom shorter than the counterion in MUV (E108). Previously, we replaced the counterion in VCOP with a glutamic acid residue (D108E), anticipating that we would convert VCOP into a UV-like pigment (*14*). However, the D108E mutation produced an only 12 nm blue shift in the λ_{max}. The D108A and D108G mutations in VCOP resulted in a dramatic change in the λ_{max} (*14*). The results led us to investigate the photoactivation properties of the VCOP-D108A pigment.

Will VCOP-D108A photoactivate without a charged residue at position 108 and with an unprotonated SB? To address this question, we have carried out a detailed

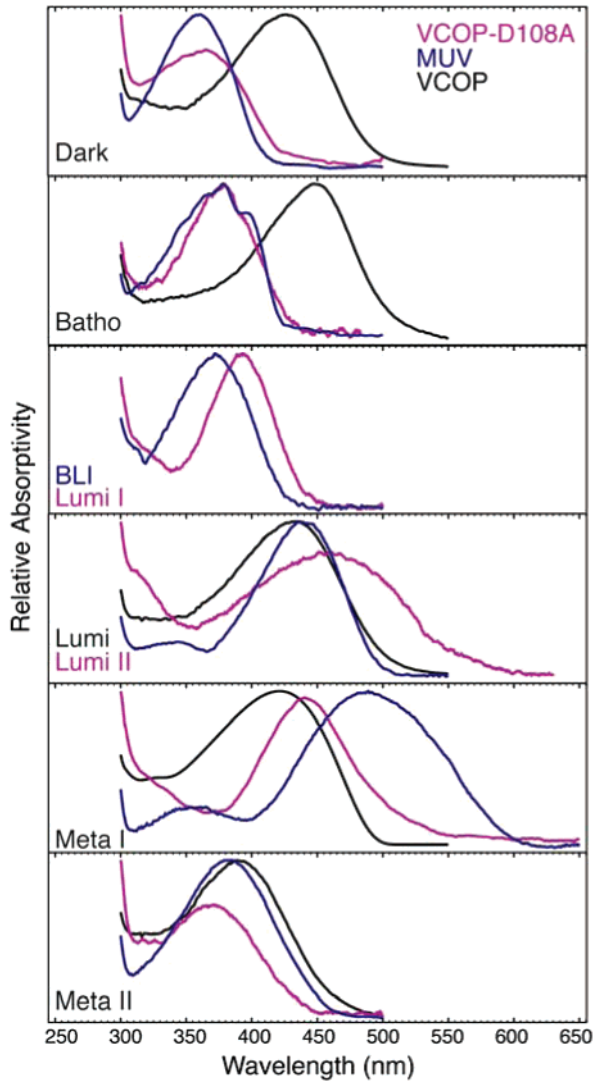

FIGURE 6: Electronic spectra of the photobleaching intermediates of VCOP, MUV, and VCOP-D108A generated via SVD spectral decomposition of the temperature-trapped photostationary state spectra. The absorption maxima are accurate to ±2 nm. Note that VCOP *batho* decays to *lumi*. MUV *batho* decays to a blue-shifted intermediate called BLI, whereas VCOP-D108A *batho* decays to a red-shifted intermediate called *lumi* I.

spectroscopic study of VCOP-D108A. The low-temperature spectroscopy experiment reveals a trappable *batho* intermediate with a λ_{max} of 380 nm. The dark → *batho* spectra of VCOP-D108A are analogous to the *batho* formation in MUV as shown in Figure 6. The intermediates after *batho* are greatly affected by the D108A substitution. Unlike the case in MUV or MUV-E108Q, the VCOP-D108A *batho* is converted to *lumi* I, accompanied by a small red shift in the chromophore band (λ_{max} = 394 nm). A gradual increase in the temperature from 180 to 200 K converts *lumi* I to *lumi* II and dramatically red shifts the absorption maximum to 460 nm. Two *lumi* intermediates, which are both red-shifted compared to the *batho* intermediate, have not been observed previously in other vertebrate opsins. In most cases, a blue-shifted intermediate (BLI in MUV and BSI in rhodopsin) is observed after *batho* and before *lumi* (*7*, *31*, *32*). The *batho* → BSI transition in rhodopsin has been interpreted as the relaxation of the chromophore, while the BSI → *lumi* transition in rhodopsin involves protein conformational changes (*16*, *31*, *33*, *34*). In the case of VCOP-D108A, *lumi*

Table 1: Distances between the Schiff Base Nitrogen of the Chromophore and the Hydrogen Atoms of Nearby Water Molecules and Residues in VCOP-D108A[a]

protein and atoms	distance after 2 ns MD (Å)
Dark State (11-*cis*-retinal)[b]	
retinal and H_2O	
NZ(Ret)−H1	2.26
NZ(Ret)−H2	3.49
retinal and Ser-85	
NZ(Ret)−HO	4.67
retinal and Ser-181	
NZ(Ret)−HO	2.65
Lumi I (all-*trans*-retinal)[b]	
retinal and H_2O	
NZ(Ret)−H1	2.81
NZ(Ret)−H2	3.56
retinal and Ser-85	
NZ(Ret)−HO	5.21
retinal and Ser-181	
NZ(Ret)−HO	7.70

[a] The distances between the Schiff base nitrogen of the retinal [NZ(ret)] and the hydrogen atoms of Ser-85, Ser-181, and nearby water molecule were measured. The water molecule closest to the SB was selected. [b] The retinal chromophore in the models has an unprotonated SB.

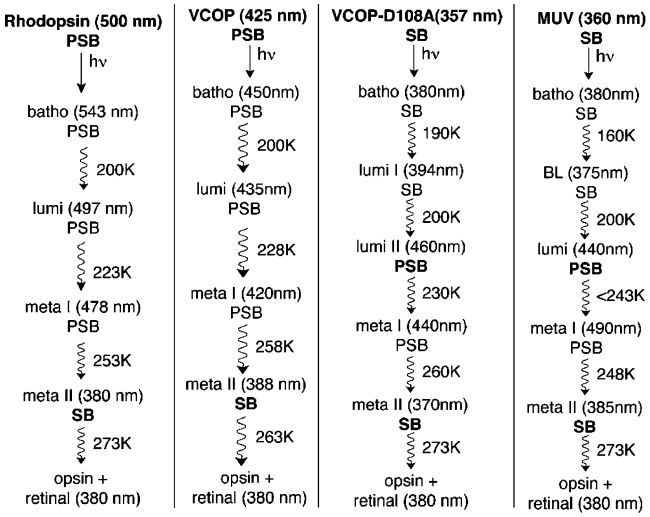

FIGURE 7: Comparison of the photoactivation sequences of rhodopsin, MUV, VCOP, and VCOP-D108A based on low-temperature experiments. The data for the photobleaching intermediates of rhodopsin, VCOP, and MUV are from previous studies (*7*, *31*, *43*).

I (λ_{max} = 394 nm) has a red-shifted absorption maximum compared to that of *batho*, which can be trapped at <200 K. Formation of *lumi* I via thermal decay of the *batho* intermediate could be interpreted as a structural rearrangement of the protein. At *lumi* I (λ_{max} = 394 nm), the SB is still unprotonated, but opsin movement could be detected in the aromatic region (~280 nm) of the absorbance spectrum of the *batho* → *lumi* transition (Figure 2A). Evidently, changes in the interactions between the SB and nearby residues or water molecule could lead to the *lumi* I red shift. The ~65 nm spectral shift in the absorbance spectra toward the red during the formation of *lumi* II in VCOP-D108A infers that the SB becomes protonated during the *lumi* I → *lumi* II transition. *Meta* I decays to *meta* II at >230 K, with an apparently normal path, unlike the formation of an aberrant *meta* I in the MUV-E108Q counterion variant (*4*). The results for VCOP-D108A support the notion that proper

Table 2: Spectroscopic Properties of the Chromophore in Wild-Type VCOP and VCOP-D108A as a Function of Binding Site Environment[a]

VCOP (exp λ_{max} = 425 nm)			VCOP-D108A (exp λ_{max} = 357 nm)		
property	residues included in calculation	value (nm)	property	residues included in calculation	value (nm)
ΔE (S1)	LYR	595 $f = 0.38$	ΔE (S2)	LYR[b]	371 $f = 1.30$
ΔE (S1)	LYR, S85, D108	417 $f = 0.54$	ΔE (S2)	LYR,[b] S85, A108	371 $f = 1.32$
ΔE (S1)	LYR, S85, D108, E176, S181	430 $f = 0.48$	ΔE (S2)	LYR,[b] S85, A108, E176, S181	374 $f = 1.34$
ΔE (S1)	LYR, S85, D108, E176, S181, H_2O within 4 Å	413 $f = 0.57$	ΔE (S2)	LYR,[b] S85, A108, E176, S181, water within 4 Å	371 $f = 1.35$
ΔE (S1)	LYR, S85, D108, E176, S181, W186, C206, F207, Y260, S290	425 $f = 0.57$	ΔE (S2)	LYR,[b] S85, A108, E176, S181, W186, C206, F207, Y260, S290	367 $f = 1.22$

[a] The MNDO-PSDCI calculations included full single- and double-configuration interaction (CI) from the chromophore (LYR) π-system. All the data are given for the low-lying strongly allowed ^1B_u*-like excited singlet state, which is responsible for the λ_{max} absorption band. The oscillator strength (f) is also given with the calculated λ_{max}. In some calculations for VCOP-D108A, the lowest singlet state was a doubly excited ^1A_g*-like state with a relatively low oscillator strength. [b] The retinal chromophore (LYR) of the VCOP-D108A model has an unprotonated Schiff base.

Table 3: Comparison of Calculated Energies of MUV and VCOP-D108A Models

	heat of formation (kcal/mol)[a]	
models	protonated E176	charged E176
MUV	−12484.7	−12597.2
VCOP-D108A	−13728.2	−13702.4

[a] Both models contain an 11-*cis*-retinal chromophore bound to the opsin via an unprotonated SB linkage. Each model underwent 2 ns of dynamics with initial conditions altered on the basis of the protonation state of Glu-176 (see Materials and Methods). The final heat of formation was calculated by using MOZYME and a PM3 Hamiltonian.

formation of *meta* I required a *lumi* intermediate with a protonated Schiff base.

The SB in VCOP-D108A first becomes protonated in *lumi* II. Where does the proton come from? The first possible proton donor is the highly conserved amino acid in extracellular loop II, E176. This hypothesis requires that E176 be protonated in the dark state or be protonated prior to *lumi* II formation. In rhodopsin, the protonation state of this residue is still unresolved (*5*, *35*). The second possible proton source is solvent. Molecular models indicate that there could be one to two water molecules accessible to the SB. Table 1 shows the distances among the nearest water molecule to the Schiff base, selected polar residues, and the SB nitrogen. Lowering the pH from 6.8 to 5.9 increased the kinetics of *lumi* II formation, suggesting that the protonation of the SB is faster. This could indicate that E176 or the SB becomes more accessible to solvent during the transition from *lumi* I to *lumi* II. The photobleaching sequence of VCOP-D108A is compared to those of rhodopsin, VCOP, and MUV in Figure 7.

Binding Site Models. To characterize the protonation event of the chromophore in VCOP-D108A, we have generated models of the dark state of the pigments. The homology models of VCOP, MUV, and VCOP-D108A were followed by successive energy minimizations. The molecular dynamic simulations performed were identical for all pigments. Selected residues in the binding sites of both VCOP and VCOP-D108A are shown in Figure 8. Both VCOP and VCOP-D108A models predict that the chromophore has direct access to a few water molecules. We have also generated possible models of the earlier intermediates of VCOP-D108A, wherein the retinal chromophore is in the all-*trans* conformation with the protonated and unprotonated SB (not shown). Table 1 shows the distances from the SB nitrogen of the chromophore to nearby hydrogen atoms of water molecules and selected polar residues. In all the models that have been generated, the SB nitrogen of the chromophore remains in the proximity (within 3 Å) of a hydrogen atom, either from a nearby water molecule or from a polar residue in the binding site. This observation provides an explanation of how the SB becomes protonated in VCOP-D108A.

The photophysical properties of the bound chromophore in WT VCOP and VCOP-D108A were calculated by using MNDO-PSDCI molecular orbital theory. The results are presented in Table 2, which lists the calculated absorption maximum as a function of the number of binding site residues included in the calculation. Analysis of these data indicates that deprotonation of the Schiff base is the primary source of the blue shift in VCOP-D108A. Indeed, the calculations on VCOP-D108A yield absorption maxima that are very close to those predicted by MNDO-PSDCI calculations on MUV (*7*), but there is one important difference observed. In all cases, the lowest-lying singlet state in MUV is calculated to be the strongly allowed $^1B_u{}^{*+}$-like state, as in VCOP (*7*). In contrast, VCOP-D108A is calculated to have a lowest-lying $^1A_g{}^{*-}$-like state (see Table 2). We believe this difference in excited-state level ordering is responsible for the observed decrease in the relative quantum efficiency of the primary event in VCOP-D108A relative to MUV (Figure 9). Our analysis was based on the spectroscopic observation of *batho* formation and used the same methods and procedures as outlined in Kim et al. (*36*). Ratios based on the initial formation (0.872) versus photostationary state (0.869) are nearly identical, and we conclude that VCOP-D108A has a primary event quantum efficiency lower than that of MUV by 0.87 ± 0.05. The quantum mechanical origin of this difference is believed to be associated with a difference in the potential energy surfaces for photoisomerization. When the $^1B_u{}^{*+}$-like state is the lowest excited singlet state, as it is in rhodopsin and MUV, a barrierless excited-state potential surface is generated due to repulsion between

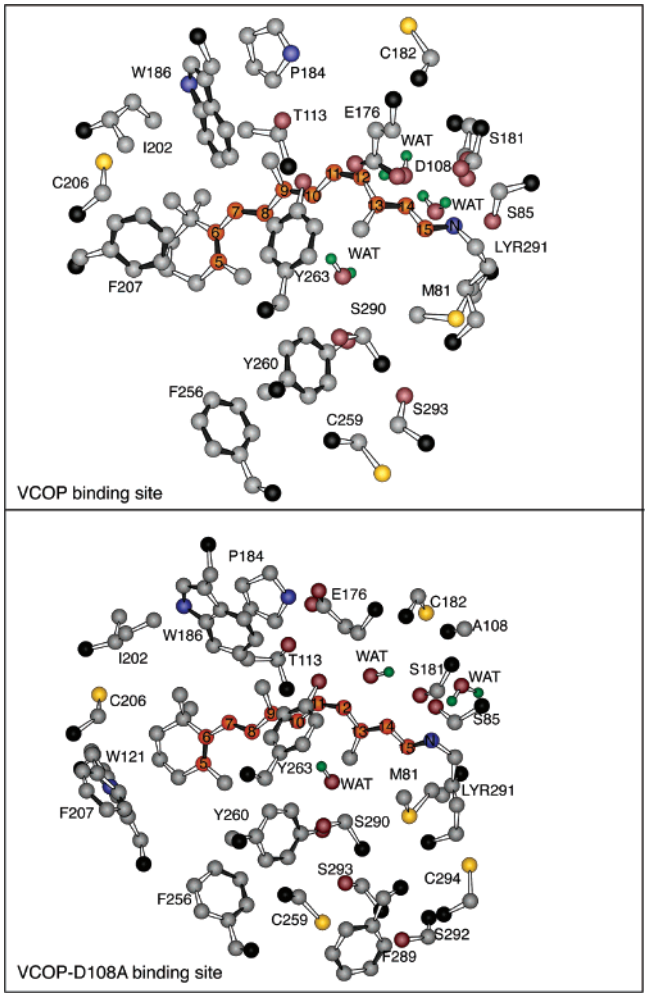

FIGURE 8: Selected VCOP and VCOP-D108A binding site residues following a 2 ns molecular dynamics simulation. The α-carbons are colored black, and the hydrogen atoms are not shown except for those on the water molecules (WAT). VCOP has a protonated SB retinal chromophore, whereas VCOP-D108A has an unprotonated SB chromophore.

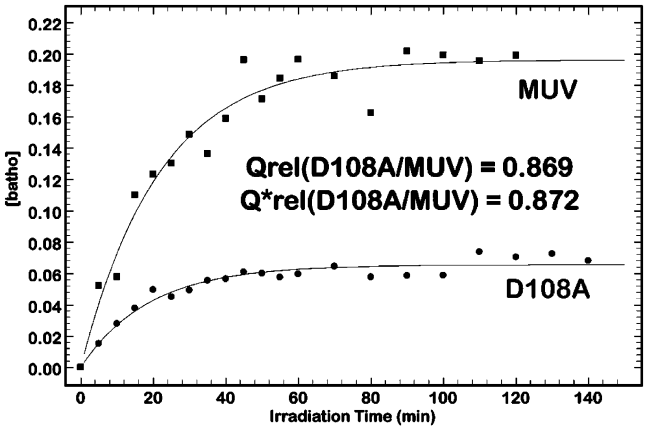

FIGURE 9: Quantum yield analysis of the primary events in MUV and VCOP-D108A based on the formation of the *batho* intermediate as a function of time. The kinetic and photostationary state analyses predict a primary event quantum efficiency in VCOP-D108A divided by that in MUV of 0.87 ± 0.05.

this state and the higher-energy $^1A_g{}^{*-}$-like state during 11-*cis* to 11-*trans* isomerization (*37*). This level ordering generates not only a barrierless photoisomerization pathway but also an interconversion pathway that is vibrationally

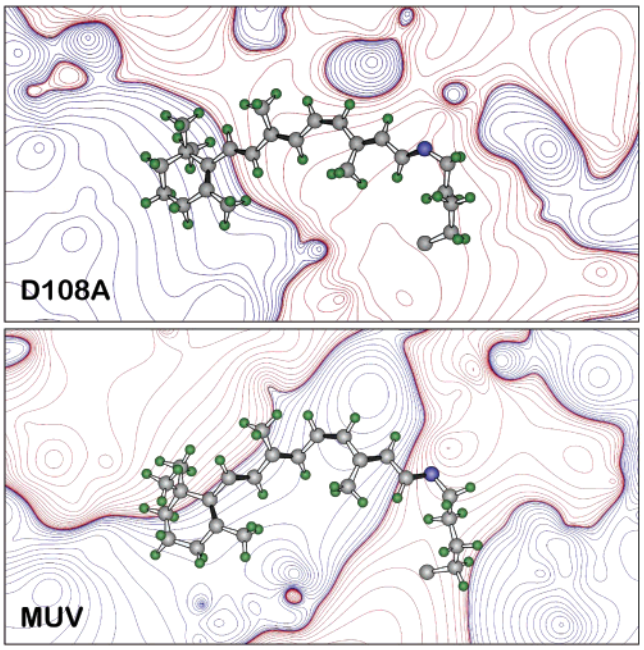

FIGURE 10: Electrostatic comparison of the binding sites of VCOP-D108A and MUV after both proteins underwent two 2 ns dynamics. The contours show the ground state electrostatic fields in the plane of the chromophore where the red contours indicate excess positive charge and the blue contours indicate excess negative charge. Charges on the atoms of the chromophore and Glu-176 were excluded.

coherent (*38*). When the lowest two excited singlet states are reversed, a small barrier is created that decreases the quantum efficiency. Two-photon studies are underway to examine level ordering in MUV and VCOP-D108A spectroscopically.

Of greater interest to this investigation is the observation of the significant difference in the photobleaching sequences of VCOP-D108A versus MUV. Both are UV pigments with unprotonated Schiff base chromophores, but as demonstrated in Figure 7, the nature of the photobleaching sequence is significantly different. VCOP-D108A has two *lumi* intermediates, a *meta* I state which is blue-shifted relative to the *lumi* II intermediate, and a *meta* II intermediate that is blue-shifted relative to all of the *meta* II intermediates observed in the other pigments (Figure 7). In contrast, MUV has a blue-shifted intermediate that is formed from the *batho* intermediate (BLI), which is roughly comparable to the blue-shifted intermediate (BSI) observed in rhodopsin. We believe the significant differences in the photobleaching sequences of VCOP-D108A versus MUV can be traced to the protonation state of Glu-176, a residue that lies above the center of the chromophore (Figure 8). MOZYME calculations indicate that Glu-176 is negatively charged in MUV but neutral (protonated) in VCOP-D108A (Table 3). This difference in the protonation state of a binding site residue generates significant differences in the electrostatic fields in the plane of the chromophores in these two pigments (Figure 10). Nevertheless, both of these pigments display one important similarity. The chromophore becomes protonated during the photobleaching sequence. We have proposed that this characteristic of UV pigments reflects the mechanistic importance of the counterion switch mechanism (*5*) to the activation process of both rhodopsin and cone pigments (*6*, *7*), but in the case of the UV pigments, which uniformly

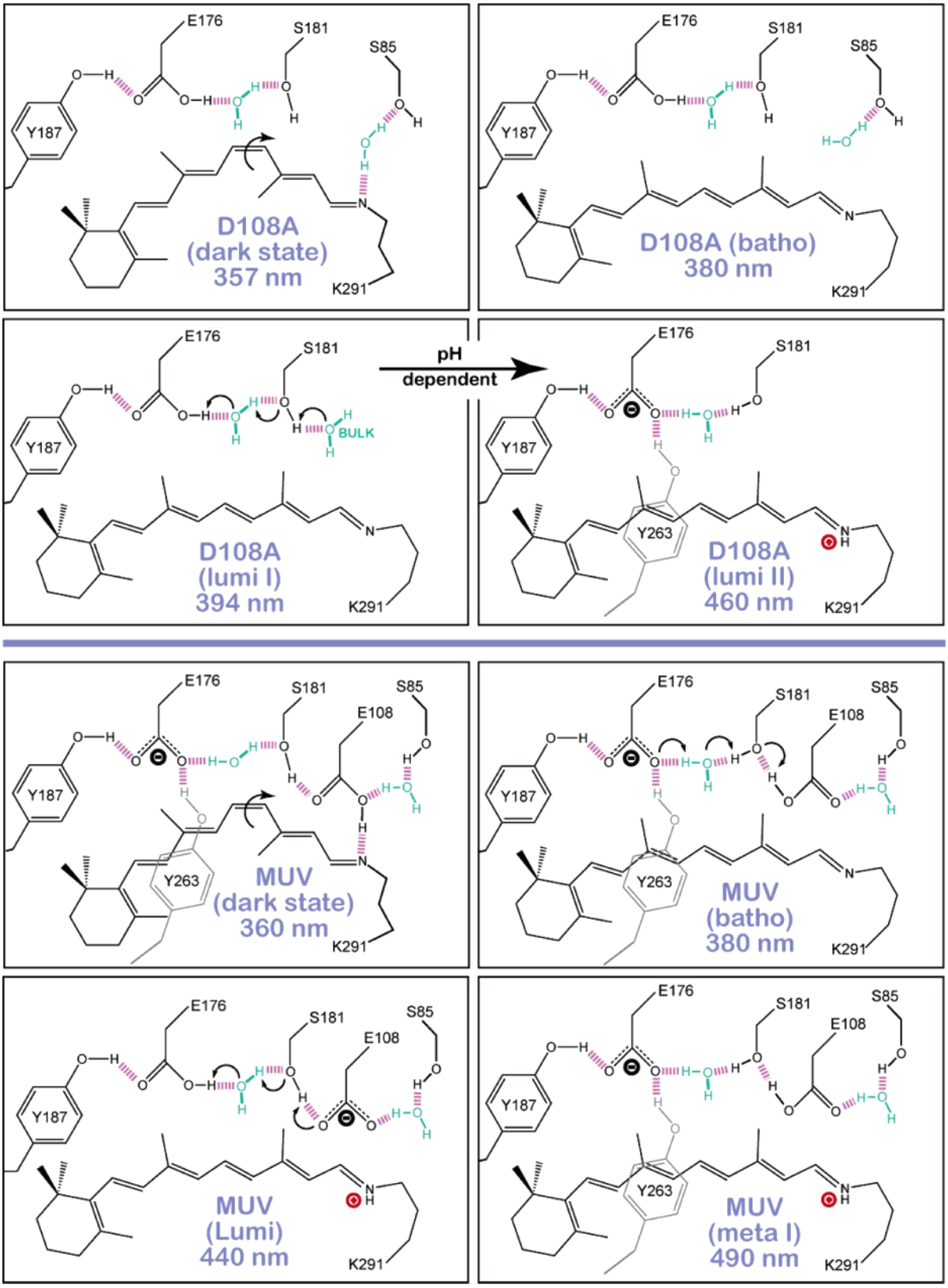

FIGURE 11: Schematic models of the early photobleaching intermediates of MUV and VCOP-D108A based on reconciliation of our spectroscopic and theoretical studies (see the text). The arrows in the dark state indicate conformational changes associated with the transformation from the dark to the *batho* intermediate in MUV and VCOP-D108A. The positions of the key residues surrounding the chromophore are approximate and based on the molecular models that were generated. The atoms included in the scheme are possible key residues in the protonation of the SB in both MUV and VCOP-D108A. Spectroscopic studies show that the VCOP-D108A *lumi* I to *lumi* II transformation is pH-dependent and involves the protonation of the SB. As for the MUV pigment, the protonation occurs during *batho* to *lumi* transformation together with a large red shift. The MUV model is based on the assumption that a counterion switch occurs during the *lumi* to *meta* I transformation (*7*, *8*).

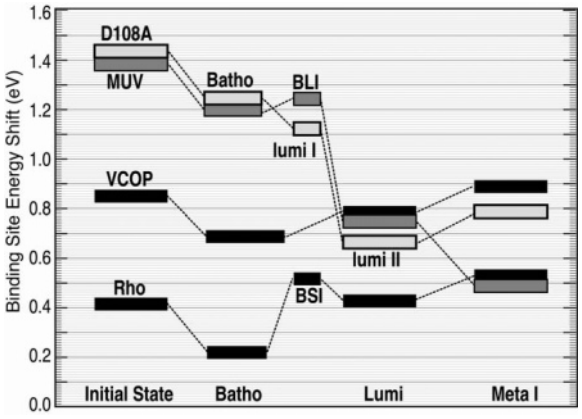

FIGURE 12: Protein-induced blue shifts associated with incorporation of the Schiff base or protonated Schiff base chromophores into the binding sites of the dark states and early intermediates of rhodopsin (Rho), the violet cone opsin of *Xenopus* (VCOP), mouse UV (MUV), and VCOP-D108A. The shift is calculated by assuming that an isolated all-*trans* protonated Schiff base chromophore has an absorption maximum of 600 nm.

exhibit a deprotonated Schiff base chromophore in the dark state, the counterion switch process is complicated by the fact that the chromophore must become protonated to interact with the secondary counterion. The observation that VCOP-D108A and MUV have different protonation states for Glu-176 in the dark provides an interesting challenge to provide a realistic molecular model of the photobleaching processes in these two proteins. Our proposed schemes are shown in Figure 11. Although these schemes are consistent with the observed absorption maxima, other possibilities exist, and further work will be required to accurately assign the nature of these intermediates.

What remains is to examine the relevance of these observations to the photobleaching processes of visual pigments in general. Binding site-induced shifts of the chromophores in the intermediates of rhodopsin, MUV, VCOP, and VCOP-D108A are compared in Figure 12. The shifts are calculated using a very simple model based on the assumption that an isolated protonated Schiff base has an absorption maximum at 600 nm. The trends are the most important as they provide a simple but useful perspective on the chromophore−protein interactions during the photobleaching process. As can be observed by reference to Figure 12, the primary events in all four proteins involve a nearly identical bathochromic shift of ~0.2 eV. This represents a curious observation because it is commonly assumed that a significant portion of both the bathochromic shift and energy storage of the primary event is associated with charge separation of the positively charged chromophore from the primary counterion (*39*−*42*), but the two UV pigments with unprotonated Schiff base chromophores exhibit shifts virtually identical to those observed in the two pigments with protonated 11-*cis* chromophores. This result suggests that conformational distortion is the primary source of the bathochromic shift of the primary events in these visual pigments. The question of whether the same observation also applies to energy storage remains. To help answer this question, photocalorimetric studies of the primary event in MUV are currently in progress (*42*). Of equal importance is the observation that E176 is protonated in VCOP-D108A but deprotonated (negatively charged) in MUV (Table 3). Both pigments are able to undergo successful photoactivation, but the process in VCOP-D108A is less efficient and involves a convoluted photobleaching sequence significantly different from that observed in MUV. Our studies support the importance of having a negatively charged glutamic acid residue at position 176 in the UV pigments. The question that remains to be answered, however, is whether the homology equivalent residue in rhodopsin (E181) is also negatively charged. The state of protonation of this residue in the dark state of rhodopsin is a current subject of debate (*5*, *35*). These studies suggest, by inference, that E181 is deprotonated in rhodopsin.

COMMENTS AND CONCLUSIONS

The single-amino acid D108A substitution converts the violet cone pigment of *Xenopus laevis* (VCOP) into a functional UV pigment which photobleaches. When we compare the photophysical properties of this protein with those of the native mouse UV pigment (MUV), we find that VCOP-D108A has a less efficient primary event and undergoes a convoluted photobleaching sequence. We trace the difference to the protonation state of the glutamic acid residue that is located near the center of the chromophore polyene chain, E176. Nevertheless, both proteins generate a protonated chromophore during the photobleaching sequence, providing further evidence that a counterion switch (or counterion creation) is requisite for UV pigment activation. Although we do not yet fully understand the molecular details of this process, our schematics in Figure 11 provide a preliminary model. The fact that all rhodopsin and cone pigments investigated to date generate photobleacing intermediates which involve the interaction of a protonated Schiff base chromophore with a negatively charged E176 (or E181) residue suggests that visual pigments must undergo significant helical displacements during photoactivation, but contrary to intuition, studies of the UV pigments suggest that this process is not driven by an electrostatic interaction between the PSB(+) chromophore and the secondary counterion [E176(−) or E181(−)]. Rather, this interaction is created by large amplitude motion of the α-helices that translocate the Schiff base region of the chromophore closer to the secondary counterion. In the case of both rhodopsin and VCOP, the large amplitude motion creates a counterion switch. In the case of the UV pigments, the large amplitude motion generates a binding site environment that induces protonation of the chromophore. It is logical to conclude that the large amplitude motion in all of these proteins is similar. However, before we accept the counterion switch (or creation) model as being a universal feature of all visual pigments, we note that most red cones have no glutamic acid residue in this position. Rather, most red cones have a histidine residue at the homologous position 181 (*6*). Studies on the red cone pigments are needed and should provide us with new insights into the nature of the large amplitude motions that are important in the activation mechanism of the visual pigments.

REFERENCES

1. Ebrey, T., and Koutalos, Y. (2001) Vertebrate photoreceptors, *Prog. Retinal Eye Res. 20*, 49−94.
2. Yokoyama, S., and Shi, Y. (2000) Genetics and evolution of ultraviolet vision in vertebrates, *FEBS Lett. 486*, 167−172.

3. Yokoyama, S., Isenberg, K. E., and Wright, A. F. (1989) Adaptive evolution of G-protein coupled receptor genes, *Mol. Biol. Evol. 6*, 342−353.
4. Yokoyama, R., and Yokoyama, S. (1990) Convergent evolution of the red- and green-like visual pigment genes in fish, *Astyanax fasciatus*, and human, *Proc. Natl. Acad. Sci. U.S.A. 87*, 9315−9318.
5. Yan, E. C. Y., Kasmi, M. A., Ganim, Z., Hou, J. M., Pan, D., Chang, B. S. W., Sakmar, T. P., and Mathies, R. A. (2003) Retinal counterion switch in the photoactivation of the G protein-coupled receptor rhodopsin, *Proc. Natl. Acad. Sci. U.S.A. 100*, 9262−9267.
6. Birge, R. R., and Knox, B. E. (2003) Perspectives on the counterion switch-induced photoactivation of the G protein-coupled receptor rhodopsin, *Proc. Natl. Acad. Sci. U.S.A. 100*, 9105−9107.
7. Kusnetzow, A., Dukkipati, A., Babu, K. R., Ramos, L., Knox, B. E., and Birge, R. R. (2004) Vertebrate ultraviolet visual pigments: Protonation of the retinylidene Schiff base and a counterion switch during photoactivation, *Proc. Natl. Acad. Sci. U.S.A. 101*, 941−946.
8. Dukkipati, A., Kusnetzow, A., Babu, K. R., Ramos, L., Singh, D., Knox, B. E., and Birge, R. R. (2002) Phototransduction by vertebrate ultraviolet visual pigments: Protonation of the retinylidene Schiff base following photobleaching, *Biochemistry 41*, 9842−9851.
9. Cowing, J. A., Poopalasundaram, S., Wilkie, S. E., Robinson, P. R., Bowmaker, J., and Hunt, D. (2002) The molecular mechanism for the spectral shifts between vertebrate ultraviolet- and violet-sensitive cone visual pigments, *Biochem. J. 367*, 129−135.
10. Fasick, J., Applebury, M., and Oprian, D. (2002) Spectral tuning in the mammalian shortwavelength sensitive cone pigments, *Biochemistry 41*, 6860−6865.
11. Hunt, D., Cowing, J. A., Wilkie, S. E., Parry, J. W., Poopalasundaram, S., and Bowmaker, J. (2004) Divergent mechanisms for the tuning of shortwave sensitive visual pigments in vertebrates, *Photochem. Photobiol. 3*, 713−720.
12. Yokoyama, S., Radlwimmer, F., and Blow, N. (2000) Ultraviolet pigments in birds evolved from violet pigments by a single amino acid change, *Proc. Natl. Acad. Sci. U.S.A. 97*, 7366−7371.
13. Wilkie, S. E., Robinson, P. R., Cronin, T. W., Poopalasundaram, S., Bowmaker, J. K., and Hunt, D. M. (2000) Spectral tuning of avian violet- and ultraviolet-sensitive visual pigments, *Biochemistry 39*, 7895−7901.
14. Babu, K. R., Dukkipati, A., Birge, R. R., and Knox, B. E. (2001) Regulation of phototransduction in short wavelength cone visual pigments via the retinylidene Schiff base counterion, *Biochemistry 40*, 13760−13766.
15. Vought, B. W., Dukkipati, A., Max, M., Knox, B. E., and Birge, R. R. (1999) Photochemistry of the primary event in short-wavelength visual opsins at low temperature, *Biochemistry 38*, 11287−11297.
16. Saam, J., Tajkhorshid, E., Hayashi, S., and Schulten, K. (2002) Molecular dynamics investigation of primary photoinduced events in the activation of rhodopsin, *Biophys. J. 83*, 3097−3112.
17. Okada, T., Sugihara, M., Bondar, A. N., Elstner, M., Entel, P., and Buss, V. (2004) The retinal conformation and its environment in rhodopsin in light of a new 2.2 Å crystal structure, *J. Mol. Biol. 342*, 571−583.
18. Marti-Renom, M. A., Stuart, A. C., Fiser, A., Sanchez, R., Melo, F., and Sali, A. (2000) Comparative protein structure modeling of genes and genomes, *Annu. Rev. Biophys. Biomol. Struct. 29*, 291−325.
19. Zhang, L., and Hermans, J. (1996) Hydrophilicity of cavities in proteins, *Proteins 24*, 433−438.
20. Kalé, L., Skeel, R., Bhandarkar, M., Brunner, R., Gursoy, A., Krawetz, N., Phillips, J., Shinozaki, A., Varadarajan, K., and Schulten, K. (1999) NAMD2: Greater scalability for parallel molecular dynamics, *J. Comput. Phys. 151*, 283−312.
21. Fong, S. L., Tsin, A. T., Bridges, C. D., and Liou, G. I. (1982) Detergents for extraction of visual pigments: Types, solubilization, and stability, *Methods Enzymol. 81*, 133−140.
22. Nicholls, A., Sharp, K. A., and Honig, B. (1991) Protein folding and association: Insights from the interfacial and thermodynamic properties of hydrocarbons, *Proteins 11*, 281−296.
23. Stewart, J. J. P. (1999) *MOZYME*, Fujitsu Limited, Tokyo, Japan.
24. Stewart, J. J. P. (1996) Application of localized molecular orbitals to the solution of semiempirical self-consistet field equations, *Int. J. Quant. Chem. 58*, 133−146.
25. Stewart, J. J. P. (1997) Calculation of the geometry of a small protein using semiempirical methods, *THEOCHEM*, 195−205.
26. Martin, C. H., and Birge, R. R. (1998) Reparameterizing MNDO for excited-state calculations using ab initio effective Hamiltonian theory: Application to the 2,4-pentadien-1-iminium cation, *J. Phys. Chem. A 102*, 852−860.
27. Kusnetzow, A., Singh, D. L., Martin, C. H., Barani, I., and Birge, R. R. (1999) Nature of the chromophore binding site of bacteriorhodopsin. The potential role of Arg-82 as a principal counterion, *Biophys. J. 76*, 2370−2389.
28. Ren, L., Martin, C. H., Wise, K. J., Gillespie, N. B., Luecke, H., Lanyi, J. K., Spudich, J. L., and Birge, R. R. (2001) Molecular mechanism of spectral tuning in sensory rhodopsin II, *Biochemistry 40*, 13906−13914.
29. Sakmar, T. P., Franke, R. R., and Khorana, H. G. (1989) Glutamic acid 113 serves as the retinylidene Schiff base counterion in bovine rhodopsin, *Proc. Natl. Acad. Sci. U.S.A. 86*, 8309−8313.
30. Zhukovsky, E. A., and Oprian, D. D. (1989) Effect of carboxylic acid side chains on the absorption maximum of visual pigments, *Science 246*, 928−931.
31. Kliger, D. S., and Lewis, J. W. (1995) Spectral and kinetic characterization of visual pigment photointermediates, *Isr. J. Chem. 35*, 289−307.
32. Jäger, S., Lewis, J. W., Zvyaga, T. A., Szundi, I., Sakmar, T. P., and Kliger, D. S. (1997) Time-resolved spectroscopy of the early photolysis intermediates of rhodopsin Schiff base counterion mutants, *Biochemistry 36*, 1999−2009.
33. Jager, S., Lewis, J. W., Zvyaga, T. A., Szundi, I., Sakmar, T. P., and Kliger, D. S. (1997) Chromophore structural changes in rhodopsin from nanoseconds to microseconds following pigment photolysis, *Proc. Natl. Acad. Sci. U.S.A. 94*, 8557−8562.
34. Pan, D., Ganim, Z., Kim, J. E., Verhoeven, M. A., Lugtenburg, J., and Mathies, R. A. (2002) Time-resolved resonance Raman analysis of chromophore structural changes in the formation and decay of rhodopsin's BSI intermediate, *J. Am. Chem. Soc. 124*, 4857−4864.
35. Ludeke, S., Beck, M., Yan, E. C. Y., Sakmar, T. P., Siebert, F., and Vogel, R. (2005) The role of Glu 181 in the photoactivation of rhodopsin, *J. Mol. Biol. 353*, 345−356.
36. Kim, J. E., Tauber, M. J., and Mathies, R. A. (2001) Wavelength-dependent cis−trans isomerization in vision, *Biochemistry 40*, 13774−13778.
37. Tallent, J. R., Hyde, E. Q., Findsen, L. A., Fox, G. C., and Birge, R. R. (1992) Molecular dynamics of the primary photochemical event in rhodopsin, *J. Am. Chem. Soc. 114*, 1581−1592.
38. Wang, Q., Schoenlein, R. W., Peteanu, L. A., Mathies, R. A., and Shank, C. V. (1994) Vibrationally coherent photochemistry in the femtosecond primary event of vision, *Science 266*, 422−424.
39. Cooper, A. (1979) Energy uptake in the first step of visual excitation, *Nature 282*, 531−533.
40. Schick, G. A., Cooper, T. M., Holloway, R. A., Murray, L. P., and Birge, R. R. (1987) Energy storage in the primary photochemical events of rhodopsin and isorhodopsin, *Biochemistry 26*, 2556−2562.
41. Honig, B., Ebrey, T., Callender, R. H., Dinur, U., and Ottolenghi, M. (1979) Photoisomerization, energy storage, and charge separation: A model for light energy transduction in visual pigments and bacteriorhodopsin, *Proc. Natl. Acad. Sci. U.S.A. 76*, 2503−2507.
42. Birge, R. R., and Vought, B. W. (2000) Energetics of rhodopsin photobleaching: Photocalorimetric studies of energy storage in the early and later intermediates, in *Methods in Enzymology* (Palczewski, K., Ed.) pp 143−163, Academic Press, New York.
43. Kusnetzow, A., Dukkipati, A., Babu, K. R., Singh, D., Vought, B. W., Knox, B. E., and Birge, R. R. (2001) The Photobleaching Sequence of a Short-Wavelength Visual Pigment, *Biochemistry 40*, 7832−7844.

BI700138G